Animate124: Animating One Image to 4D Dynamic Scene

Yuyang Zhao[1], Zhiwen Yan[1], Enze Xie[2✉], Lanqing Hong[2], Zhenguo Li[2], Gim Hee Lee[1]
[1] National University of Singapore
[2] Huawei Noah's Ark Lab
https://animate124.github.io/

Figure 1. To the best of our knowledge, our **Animate124** is the first framework to animate one in-the-wild image into 3D video with the motion defined by text prompt.

Abstract

*We introduce Animate124 (**Animate-one**-image-**to-4D**), the first work to animate a single in-the-wild image into 3D video through textual motion descriptions, an under-explored problem with significant applications. Our 4D generation leverages an advanced 4D grid dynamic Neural Radiance Field (NeRF) model, optimized in three distinct stages using multiple diffusion priors. Initially, a static model is optimized using the reference image, guided by 2D and 3D diffusion priors, which serves as the initialization for the dynamic NeRF. Subsequently, a video diffusion model is employed to learn the motion specific to the subject. However, the object in the 3D videos tends to drift away from the reference image over time. This drift is mainly due to the misalignment between the text prompt and the reference image in the video diffusion model. In the final stage, a personalized diffusion prior is therefore utilized to address the semantic drift. As the pioneering image-text-to-4D generation framework, our method demonstrates significant advancements over existing baselines, evidenced by comprehensive quantitative and qualitative assessments.*

✉ Corresponding author.

1. Introduction

Generative models have recently achieved significant advancements in producing 2D images [34, 35, 37] and videos [23, 39, 51]. The creation of 3D content [30, 31, 33], a critical representation of the real world, has garnered increasing attention and has shown rapid development. Empowered by robust priors from both 2D and 3D diffusion models, the generation of 3D scenes [11, 19, 25, 30, 41] from text prompts or single images is now feasible and has witnessed remarkable progress. However, most existing research concentrates on static scenes and often overlooks the dynamic nature of the real world.

In contrast, dynamic 3D scenes (or 3D videos) more effectively represent the richly informative 3D world, offering significant applications in video games, augmented reality, and virtual reality. Despite its importance, 3D video generation remains relatively unexplored partly due to the underdevelopment in video generation models. MAV3D [41] represents a pioneering effort in generating 3D videos from text prompts. It employs temporal Score Distillation Sampling (SDS) [30] to transfer knowledge from a text-to-video diffusion model [39] into a dynamic NeRF representation [4]. However, content generation solely from

1

text often lacks control despite its diversity. This limitation has inspired the integration of various conditioning signals in 2D [13, 47, 50] and image-based conditioning in 3D [25, 31, 49]. In the realm of controllable video generation, the technique of conditioning on an initial image to guide subsequent motion [7, 47] has become both effective and popular. For example, generating a scene based on the prompt: "A panda is dancing", users may wish to define the appearance and starting pose of the panda by providing a reference image.

In this paper, we explore image-text-based 3D video generation having inspired by text-to-3D-video and controllable video generation. Guided by the motion outlined in a text prompt, our approach aims to lift and animate a single input image into a 3D video. To achieve this goal with limited input, we utilize Score Distillation Sampling (SDS) [30] to infuse knowledge from diffusion priors into a dynamic NeRF model. This implies that an efficient and effective NeRF model is essential for representation. MAV3D employs HexPlane [4] to map the X, Y, Z, and time axes onto six 2D planes and subsequently fusing these features to determine density and color. Nonetheless, we risk falling into the Janus problem with a naive adoption of MAV3D since we only have a single reference image as both a condition and a source of supervision. Specifically, the Janus problem happens when the camera direction of the reference image view is perpendicular to one of the 2D planes in HexPlane. As a consequence, the plane features overfit to the reference image, where both the front and back views resemble the reference image without a proper 3D geometry. Moreover, we empirically observe some traces of the Janus problem even when the reference image is off-perpendicular the 2D planes in HexPlane. Refer to Appendix. B for a detailed discussion and visualization of the results of HexPlane. We address these challenges by adopting a robust 4D grid feature encoding model that is capable of representing spatio-temporal information. This model predicts color and density using features derived from the 4D grid.

To animate 3D videos from a single image, we propose a static-to-dynamic and coarse-to-fine strategy that structures the optimization of the 4D representation into three distinct stages. Initially, we develop a robust static 3D model from the reference image with 2D image diffusion prior [35] and 3D diffusion prior [19]. This static model serves as the initialization of the dynamic model, from which the 3D video animation emerges. In the second stage, we employ a video diffusion prior [46] to generate the motion across various timesteps and camera perspectives. During this stage, the reference image is instrumental in aligning the first frame with the source image. However, a challenge arises as the object in the 3D video tends to drift away from the reference image over time. This drift is largely attributed to the reference image influencing only the initial frame, while subse-

quent frames primarily rely on the knowledge gained from the video diffusion model.

Personalized modeling techniques [9, 36] are effective for aligning reference images with diffusion priors. However, these methods cannot be applied to video diffusion model when only a single image instead of a video is provided. The semantic drift of video diffusion therefore seems to be inevitable. Nevertheless, personalized modeling based on a single image is feasible for image diffusion priors, and a video can be conceptualized as a sequence of consecutive images. Consequently, in the third stage of our approach, we employ frame-level processing with personalized modeling to counteract semantic drift. Specifically, this stage focuses on refining the details and appearance of the 3D video, while preserving its structure and motion. We utilize ControlNet-Tile [50] diffusion prior with the second stage 3D video as a condition. Textual Inversion [9] is employed for personalized modeling. Additionally, the ControlNet-Tile diffusion prior not only compensates for reference information but also enhances the video's resolution, as it can be applied effectively to resized low-resolution images. Through the three-stage optimization process that is powered by robust 2D and 3D diffusion priors, our **Animate124** is capable of generating realistic and diverse 3D videos. Our contributions are summarized as follows:

- We introduce Animate124, a novel framework for animating a single image into a 3D video, utilizing a 4D grid dynamic NeRF representation.
- We propose a static-to-dynamic and coarse-to-fine strategy to optimize the 4D representation, integrating 2D, 3D, and personalized modeling diffusion priors.
- We conduct extensive qualitative and quantitative experiments to compare Animate124 with baselines and state-of-the-art text-to-4D method (MAV3D [41]), demonstrating the superiority of our method.

2. Related Work

Dynamic Neural Rendering. In our framework, we employ Neural Radiance Fields (NeRFs) [26] to represent the 4D spatio-temporal scenes. NeRFs [26] enable the rendering of images from diverse target viewpoints by modeling a 3D scene through a neural network that interprets spatial coordinates. The architecture of neural network varies, extending from basic MLPs (Multilayer Perceptrons) [1, 26] to more complex voxel grid features [27, 42]. Regarding dynamic NeRFs for 4D spatio-temporal scenes, one popular approach involves separately learning a canonical field and a deformation field across different network layers. However, this technique faces challenges when dealing with changes in scene topology. Another prevailing method decomposes the spatio-temporal dimension into multiple planes [4, 8, 38], but this plane-based approach tends to result in the Janus problem when generating 3D video from a

single reference image. To overcome these limitations, inspired by Park *et al.* [29], we leverage a 4D grid model to effectively represent dynamic 3D scenes, thereby facilitating the animation of a single image into a 3D video.

Text-to-3D Generation. The evolution of multimodal foundation models [32, 35, 37] has led to significant advancements in in-the-wild text-to-3D generation. Initial efforts [12, 14, 16] focused on aligning text prompts with rendered images using CLIP [32]. Recognizing the detailed semantic capabilities of diffusion models, DreamFusion [30] and SJC [45] introduced techniques to distill knowledge from text-based diffusion models into 3D representations, yielding promising outcomes. Subsequently, more advanced methods [6, 17, 48] have emerged to further refine diffusion-based 3D generation, incorporating mesh representation and distribution optimization. In the realm of dynamic scenes, MAV3D [41] has been developed to optimize a dynamic NeRF representation through a static-to-dynamic strategy.

Image-to-3D Generation. Lifting a single image to 3D assets plays a crucial role in 3D content creation. Initial research in this area focused on domain-specific 3D lifting, employing strong domain priors for specific subjects like human bodies [21, 24] and faces [2, 3]. Recently, the emergence of potent diffusion priors has enabled the realization of in-the-wild image-to-3D generation. One prominent approach [18–20] involves fine-tuning 2D image generation models to produce multi-view images directly. Alternatively, some methods [25, 31, 44] combine 2D diffusion with the above fine-tuned multi-view 3D diffusion to optimize 3D representation by distilling diffusion knowledge. However, these techniques primarily focus on static scenes and do not incorporate aspects of animation.

Animating Single Image to Video. Image-to-video generation has gained considerable popularity in both academic circles [5, 23, 47] and commercial applications[*†]. These methods typically utilize the reference image either as the initial frame or to extract semantic information as a condition. We recognize the potential of animating the well-established static 3D scene with text, especially for applications in the metaverse and video game industries. This motivates us to pioneer the exploration of in-the-wild image-to-3D-video generation.

3. Our Method

Overview. Our framework leverages static-to-dynamic and coarse-to-fine strategy to animate a single image into a 3D video, structured in three distinct stages. Specifically, we develop a static NeRF using the reference image in the first stage (static-stage) under the guidance of both 2D and

---

3D diffusion priors. Subsequently in the second stage (coarse-stage), the 4D grid dynamic NeRF is initialized from the static NeRF and further refined with the assistance of video diffusion prior and 3D diffusion prior. In the final stage (fine-stage), we employ a personalized image diffusion prior to mitigate the semantic drift introduced by the video diffusion model. The image diffusion prior is specifically fine-tuned with the reference image to provide additional supervision. The comprehensive framework encompassing both the coarse and fine stages is illustrated in Fig. 2 with the static optimization stage excluded due to space constraints.

3.1. 4D Grid Encoding

Given a camera position and a timestep t, a ray is cast from the camera center through each pixel on the image penetrating into the scene. We sample 3D points along this ray and determine the color and density to render the image through volume rendering. Multi-scale grid encoding [27] is an efficient and effective method for storing and representing 3D scenes. The features extracted from this grid are instrumental in calculating both density and color. In the temporal domain, Fridovich-Keil *et al.* [8] have demonstrated that multi-scale grid encoding is not essential. Consequently, we construct our 4D grid in the following manner: we divide the time dimension evenly into T grids, and for each time grid, we establish a 3D multi-scale grid V (excluding hash encoding). Spatio-temporal features $F_{x,y,z,t}$ are then linearly interpolated from the two nearest time grids:

$$F_{x,y,z,t} = \frac{t_+ - t}{\Delta_t} V_{x,y,z,t_-} + \frac{t - t_-}{\Delta_t} V_{x,y,z,t_+}, \quad (1)$$

where x, y and z represent the spatial coordinates, and t denotes the normalized time within the range of $[0, 1]$. t_+, t_- and Δ_t refer to the nearest upper time grid, lower time grid and the time interval between two consecutive grids. Utilizing these spatio-temporal features, we are able to generate color c and density τ via projection MLPs. In line with DreamFusion [30], we generate albedo and simulate random light sources to accurately represent color.

Temporal Total Variation Loss. To effectively transmit the information from the first frame to subsequent time grids while promoting temporal smoothness, we apply a total variation (TV) loss [28] to the 3D grid V across the adjacent time dimensions:

$$\mathcal{L}_{TV} = \sum_{t=0}^{T-1} \sum_{x,y,z} (V_{x,y,z,t} - V_{x,y,z,t+1})^2. \quad (2)$$

3.2. Static Scene Optimization

Following Magic123 [31], we employ Score Distillation Sampling (SDS) losses from both 2D and 3D diffusion priors to guide the optimization of the static scene. This strat-
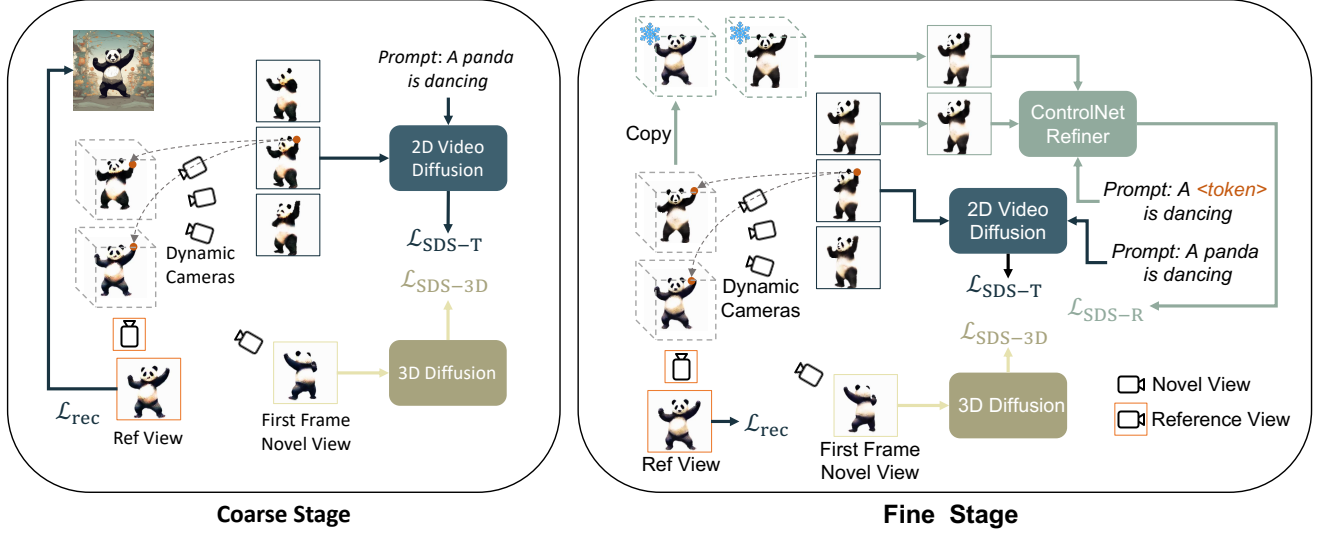
Coarse Stage   **Fine Stage**

Figure 2. The overall framework of our Animate124. After learning the static scene (the first stage, not shown in the figure), the dynamic scene is optimized with a coarse-to-fine strategy in two stages. In the coarse stage, we optimize the dynamic NeRF with the combination of video diffusion and 3D diffusion priors. Subsequently, in the fine stage, additional ControlNet prior is introduced to refine the details and correct semantic drift. The condition of ControlNet derives from the frozen coarse stage model to reduce error accumulation.

egy effectively enhances both texture quality and 3D geometry. Specifically, stable diffusion [35] conditioned on the text prompt e is adopted as 2D diffusion prior and Zero-1-to-3-XL [19] conditioned on the reference image $\tilde{\mathbf{I}}^r$ and relative pose Δp is adopted as 3D diffusion prior. The SDS loss is formulated as:

$$
\begin{aligned}
\mathcal{L}_{\text{SDS}} = \mathbb{E}_{\sigma,p,\epsilon} & \left[\omega(\sigma) \left(\epsilon_\phi^{2D} \left(\mathbf{I}^p; \sigma, e \right) - \epsilon \right) \frac{\partial \mathbf{I}^p}{\partial \theta_s} \right] \\
& + \lambda_{3D} \mathbb{E}_{\sigma,p,\epsilon} \left[\omega(\sigma) \left(\epsilon_\phi^{3D} \left(\mathbf{I}^p; \sigma, \tilde{\mathbf{I}}^r, \Delta p \right) - \epsilon \right) \frac{\partial \mathbf{I}^p}{\partial \theta_s} \right],
\end{aligned}
\tag{3}
$$

where θ_s represents the parameters of the static NeRF model and $\mathbf{I}^p$ is the rendered RGB image from the camera position p. $\epsilon_\phi^{2D}(\cdot)$ and $\epsilon_\phi^{3D}(\cdot)$ denote the predicted noise by 2D and 3D diffusion priors, respectively. $\omega(\sigma)$ refers to a weighting function corresponding to the noise timestep σ.

Additionally, we leverage the RGB $\tilde{\mathbf{I}}^r$, foreground mask $\tilde{M}^r$ and depth $\tilde{d}^r$ from the reference image to further refine the model from the reference view:

$$
\begin{aligned}
\mathcal{L}_{\text{rec}} = & \lambda_{rgb} || \tilde{M}^r \odot (\tilde{\mathbf{I}}^r - \mathbf{I}^r) || + \lambda_{mask} || \tilde{M}^r - M^r || \\
& + \lambda_d \left[1 - \frac{\text{cov} \left(\tilde{M}^r \odot \tilde{d}^r, \tilde{M}^r \odot d^r \right)}{\text{std} \left(\tilde{M}^r \odot \tilde{d}^r \right) \text{std}(\tilde{M}^r \odot d^r)} \right],
\end{aligned}
\tag{4}
$$

where λ_{rgb}, λ_{mask} and λ_d denote the weights of RGB, mask and depth loss. $\odot$ denotes Hadamard product. cov and std denote covariance and standard deviation, respectively. The static scene is optimized by the combination of the above two losses:

$$
\mathcal{L}_{\text{static}} = \mathcal{L}_{\text{SDS}} + \mathcal{L}_{\text{rec}}.
\tag{5}
$$

3.3. Coarse Dynamic Scene Optimization

The dynamic NeRF is initialized from the static NeRF. Specifically, each 3D multi-scale grid V within the T time grids is initialized with the parameters of the static model. All the time grids share the same projection layers that were pre-trained in the static stage. The dynamic model is thus initialized as a model that can generate 3D video where each frame is the same static scene. We then optimize it to align with the motion described by the text prompt e. We distill latent video diffusion model [46] with SDS loss [30, 41] to achieve this goal. Specifically, given the camera trajectory $r(t)$ of a video with a fixed number of frames N_f, we can cast rays and sample timesteps based on the frame rate. Subsequently, a video $\mathbf{V}^{r(t)}$ is rendered from the dynamic NeRF and fed into the video diffusion prior to for SDS loss:

$$
\mathcal{L}_{\text{SDS-T}} = \mathbb{E}_{\sigma, r(t), \epsilon} \left[\omega(\sigma) \left(\epsilon_\phi^{Vid} \left(\mathbf{V}^{r(t)}; \sigma, e \right) - \epsilon \right) \frac{\mathbf{V}^{r(t)}}{\partial \theta_d} \right],
\tag{6}
$$

where θ_d is the model parameters and $\epsilon_\phi^{Vid}(\cdot)$ denotes the predicted noise by the video diffusion prior.

Temporal Balanced Sampling. Unlike static 3D scenes, dynamic scenes necessitate sampling frames over a temporal range of $t \in [0, 1]$. MAV3D utilizes Make-A-Video [40] as its diffusion prior, which can condition on the video frame rate. However, this model is not publicly available. Consequently, we adopt ModelScope [46] as our video diffusion prior. ModelScope is not trained for extremely high frame rates and also lacks the capability to condition on the frame rate. To mitigate issues related to extreme frame rates, we limit the FPS (frames per second) to a range of
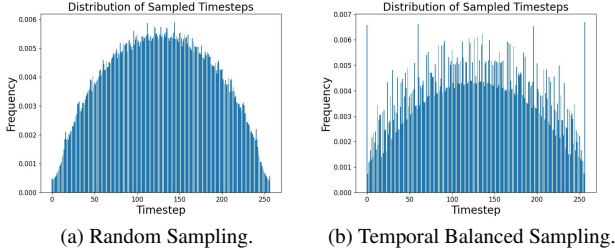
4

(a) Random Sampling.　　(b) Temporal Balanced Sampling.

Figure 3. Distribution of the sampled timestep.

$[16, 256]$. At each iteration, we sample N_f timesteps from a randomly chosen starting timestep and FPS. The distribution of sampled timesteps is depicted in Fig. 3a. However, random sampling tends to result in the beginning and ending timesteps being less frequently sampled compared to the middle timesteps, leading to suboptimal optimization of the first and last time grids (examples are provided in Appendix. D). Moreover, as the reference image constitutes the first frame of the generated video, it is beneficial to sample more from the first frame to retain the reference information. As a result, we allocate a higher probability of α specifically for sampling timesteps that begin at time 0 (the first frame), and similarly, a probability of α for timesteps concluding at time 1. The distribution of this temporal balanced sampling method is illustrated in Fig. 3b.

First Frame Supervision. Since we animate the reference image to a 3D video, the reference image, which serves as the first frame, offers additional supervision for the video generation process. Specifically, we enhance the supervision of the dynamic NeRF by incorporating both the reconstruction loss $\mathcal{L}_{\text{rec}}$ (as detailed in Eq. 4) and the 3D diffusion prior SDS loss $\mathcal{L}_{\text{SDS}-3\text{D}}$:

$$\mathcal{L}_{\text{SDS}-3\text{D}} = \mathbb{E}_{\sigma,p,\epsilon} \left[\omega(\sigma) \left(\epsilon_\phi^{3D} \left(\mathbf{V}_0^{r(t)}; \sigma, \tilde{\mathbf{I}}^r, \Delta p \right) - \epsilon \right) \frac{\partial \mathbf{V}_0^{r(t)}}{\partial \theta_d} \right],$$
(7)

only on the first frames of the sampled videos $\mathbf{V}_0^{r(t)}$, which occurs with an approximate probability of α. The final loss is thus formulated as:

$$\mathcal{L}_{\text{dynamic}} = \mathcal{L}_{\text{SDS}-\text{T}} + \lambda_{TV} \mathcal{L}_{\text{TV}} \\ + \mathbb{1}_{t_0=0}(\mathcal{L}_{\text{rec}} + \lambda_{3D} \mathcal{L}_{\text{SDS}-3\text{D}}),$$
(8)

where $\mathcal{L}_{\text{TV}}$ denotes the total variation loss (Eq. 2) and λ_{TV} is the weight for this loss.

3.4. Semantic Refinement

During the coarse dynamic scene optimization stage, information from the reference image is exclusively applied to the first frame. Details of the objects in subsequent frames are derived solely from the video diffusion prior and guided by the text prompt e. For example, in a scenario where a "panda" is animated to dance, frames beyond the first are

likely to distill a "panda" representation from the video diffusion prior that is potentially different from the reference image. Consequently, semantic drift becomes inevitable in the coarse stage.

In image-to-3D generation, personalized modeling [9, 36] is commonly used to represent the reference image in the text-to-image model. RealFusion [25] utilizes a unique token learned through textual inversion [9] to represent the reference image in the text-to-image diffusion prior. DreamCraft3D [43] optimizes the text-to-image diffusion prior using augmented renderings of the reference image, as facilitated by DreamBooth [36]. However, a single image is insufficient to learn a personalized model or token for a text-to-video diffusion prior. As a solution, we approach each frame independently and optimize it using the personalized text-to-image diffusion prior. Utilizing a naive text-to-image (T2I) personalized model can introduce unexpected motion changes since the T2I model lacks awareness of the other frames. Our objective is to have the T2I model concentrated solely on refining textures and details. To this end, ControlNet-Tile [50] is an ideal diffusion prior as it conditions on a low-resolution image while refining details and enhancing resolution. Accordingly, we learn a token to represent the reference image for the base model of ControlNet (Stable Diffusion v1.5) and optimize individual frames $\mathbf{I}_t^{r(t)}$ with this token. To prevent error accumulation, the conditioning image $\hat{\mathbf{I}}_t^{r(t)}$ is generated from the fixed dynamic NeRF model established in the coarse stage. This diffusion prior also guides the dynamic NeRF through SDS loss, which is formulated as follows:

$$\mathcal{L}_{\text{SDS}-\text{R}} = \mathbb{E}_{\sigma,r(t),\epsilon} \left[\omega(\sigma) \left(\epsilon_\phi^{CN} \left(\mathbf{I}_t^{r(t)}; \sigma, \hat{\mathbf{I}}_t^{r(t)}, e \right) - \epsilon \right) \frac{\mathbf{I}_t^{r(t)}}{\partial \theta_d} \right],$$
(9)

where θ_d is the parameters of the dynamic NeRF model and $\epsilon_\phi^{CN}(\cdot)$ denotes the predicted noise by the personalized ControlNet diffusion prior. The video and 3D diffusion priors are also leveraged in this stage, so the final loss is:

$$\mathcal{L}_{\text{refine}} = \mathcal{L}_{\text{SDS}-\text{T}} + \lambda_R \mathcal{L}_{\text{SDS}-\text{R}} + \lambda_{TV} \mathcal{L}_{\text{TV}} \\ + \mathbb{1}_{t_0=0}(\mathcal{L}_{\text{rec}} + \lambda_{3D} \mathcal{L}_{\text{SDS}-3\text{D}}),$$
(10)

where $\mathcal{L}_{\text{SDS}-\text{T}}$, $\mathcal{L}_{\text{TV}}$, $\mathcal{L}_{\text{rec}}$ and $\mathcal{L}_{\text{SDS}-3\text{D}}$ denote the video diffusion SDS loss (Eq. 6), total variation loss (Eq. 2), first frame reconstruction loss (Eq. 4) and first frame 3D diffusion SDS loss (Eq. 7), respectively. λ_R, λ_{TV} and λ_{3D} are the weights for ControlNet SDS loss, TV loss and 3D prior SDS loss, respectively.

Over-Saturation and Over-Smoothing. Score Distillation Sampling (SDS) [30] requires a large classifier-free guidance (CFG) scale to effectively distill knowledge from text-to-image diffusion models. This requirement arises because a large CFG scale can diminish the diversity of the T2I model, focusing more on fidelity to the given text.
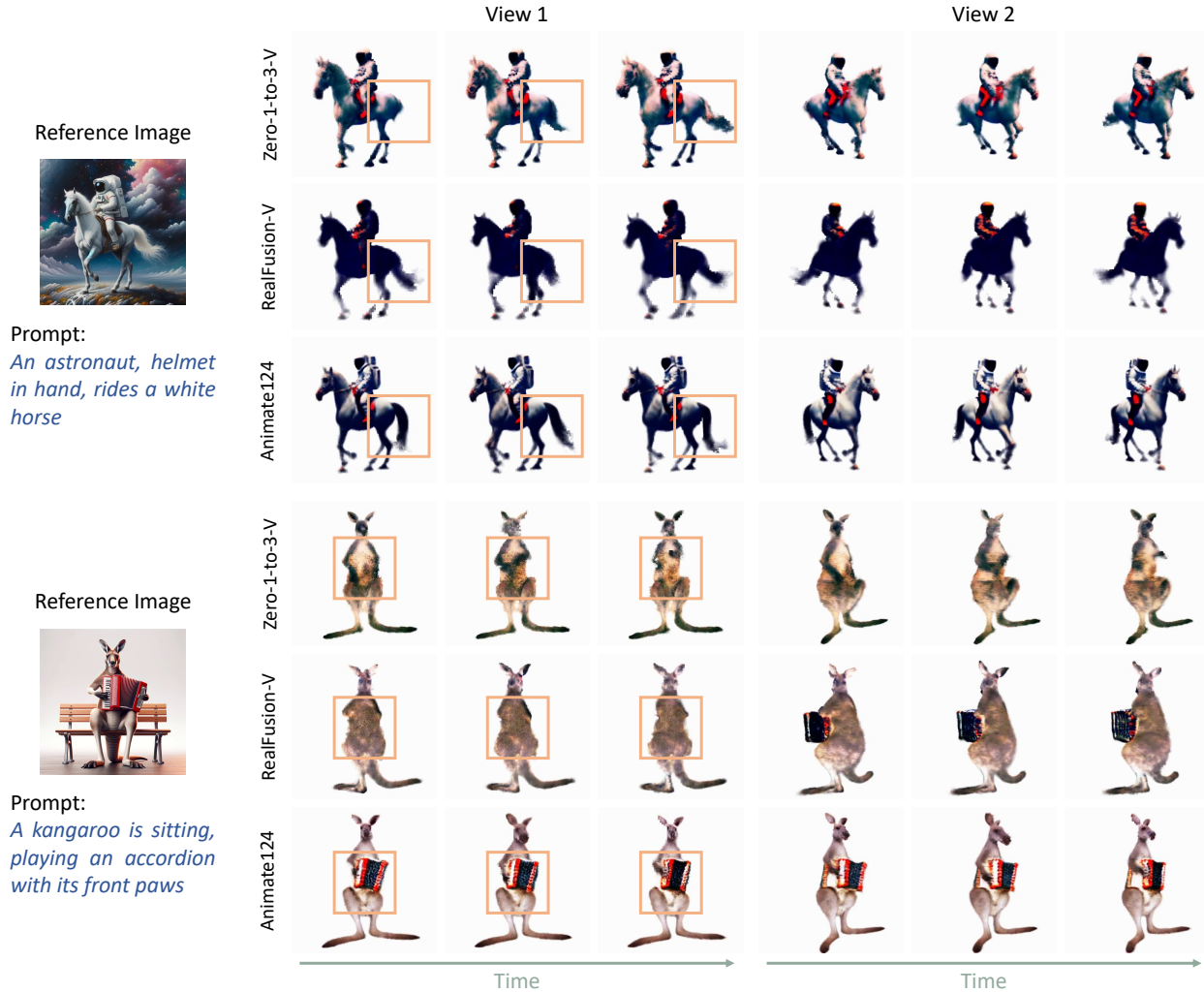
Figure 4. Qualitative comparison with the baseline methods on image-text-to-4D generation. Results in two views are shown. View 1 is the reference view and view 2 is another view. We use square in view 1 to better illustrate the motion and difference among methods.

However, as indicated by qualitative results from Dream-Fusion [30] and ProlificDreamer [48], SDS often encounters issues of over-saturation and over-smoothing due to the heightened CFG scale. Our coarse stage model faces similar challenges. ControlNet-Tile [50] conditions on a low-resolution coarse image, mirroring the effect of ancestral sampling [10, 22]. This effect allows us to use a CFG scale comparable to that in standard image generation tasks (*e.g.*, a scale of 7.5) in this diffusion prior, which can mitigate the over-saturation and over-smoothing problems observed in our coarse model.

4. Experiment

4.1. Experimental Setup

Implementation Details. In the static stage, static NeRF model is optimized for 5,000 iterations. The model con-tains 16 levels of grid encoding, with resolutions ranging from 16 to 2,048, and a dimension of 2 for each level. Two layers of MLPs with 64 hidden dimensions are used to cal-culate density and albedo. For the reference view recon-struction loss, λ_{rgb}, λ_{mask} and λ_d are set to 5, 0.5 and 0.001, respectively. Stable Diffusion v1.5 [35] and Zero-1-to-3-XL [19] serve as our 2D and 3D diffusion priors for this stage with λ_{3D} set to 40. In the coarse dynamic scene optimization stage, dynamic NeRF is optimized for 10,000 iterations with the same loss weight as in the static stage. The time grid size of dynamic NeRF is set to 64, and λ_{TV} is set to 0.1 for regularization purposes. In the semantic refinement stage, the model is further trained for 5,000 it-erations and the loss weight for ControlNet SDS loss, λ_R is adjusted to 1. Adam [15] with a learning rate 0.001 is adopted across all stages, and the rendering resolution is 128×128.

6
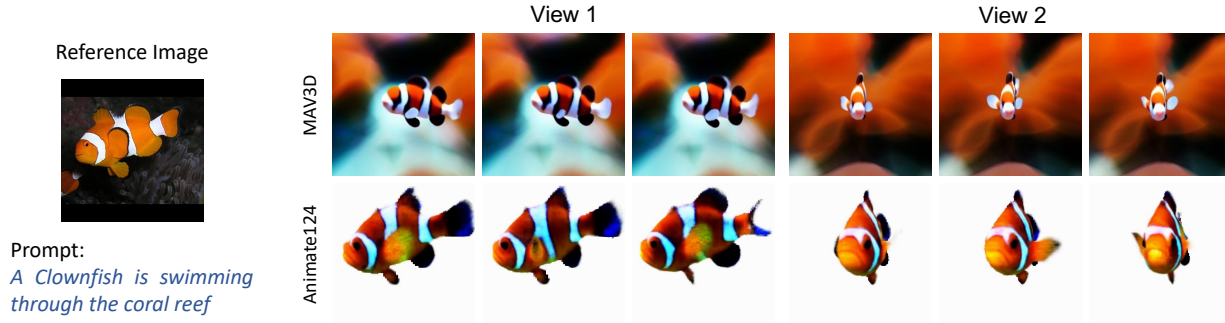
(a) Comparison with MAV3D text-to-4D generation. Reference image is not used in MAV3D. Animate124 can generate dynamic motion with the reference image as the protagonist while MAV3D cannot precisely control the subject.
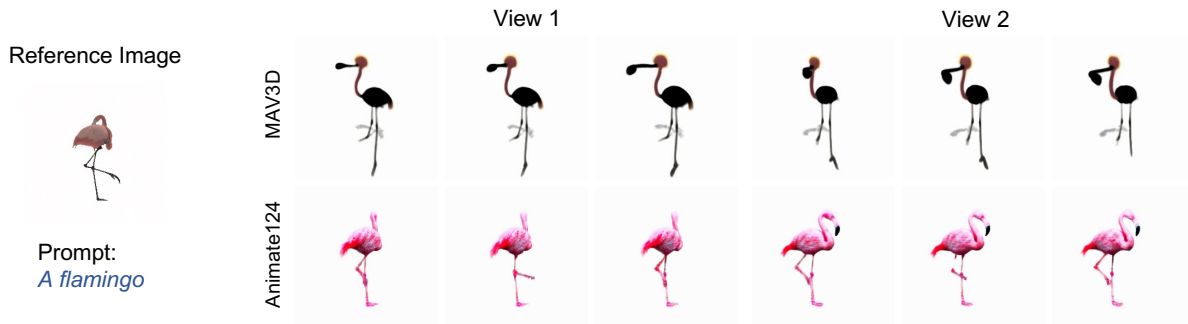
(b) Comparison with MAV3D image-to-4D generation. Text prompt is not used in MAV3D. Animate124 can better preserve the appearance and pose of the reference image.

Figure 5. Qualitative comparison with MAV3D on 4D generation with the samples on its website. **Note** that we extract frames from the videos on MAV3D website, thus the images in two views may not be perfectly matched.

Camera Setting. As for the reference view, following Magic123 [31], we assume the reference image is shot from the front view (polar angle $90°$ and azimuth angle $0°$) with the radius 1.8 meters, and the field of view (FOV) of the camera is set to $40°$. During dynamic training stages, we adopt dynamic camera [41] to simulate the camera motion in the text-to-video diffusion model.

Benchmark and Evaluation Metrics. As the first endeavor to animate a single image into a 3D video, we build a benchmark comprising 24 image-text pairs for evaluation. Our methodology is assessed across three dimensions: text-video alignment, image-video alignment, and overall video quality. For each 3D video, we render views from 10 different views around the scene. In terms of text-video alignment, we measure the retrieval accuracy of text prompts (CLIP-R [14]) and compute the image-text cosine similarity (CLIP-T) for every frame of the rendered videos. For image-video alignment, we render a video from the reference camera pose and then calculate the cosine similarity between the CLIP visual features of each frame and the reference image. Regarding video quality, we evaluate the consistency between frames by calculating the cosine similar-

ity between CLIP visual features of every two consecutive frames in each rendered video. For these assessments, we utilize the CLIP [32] ViT-B/32 variant. In addition, following MAV3D [41], we conduct user studies on five qualitative metrics: (1) similarity to the reference image; (2) faithfulness to the textual prompt; (3) video quality; (4) realism of motion; and (5) amount of motion.

4.2. Comparison with Other Methods

As the pioneering work on image-text-to-4D generation, we have developed two baselines for comparative analysis. These baselines employ distinct image-to-3D static generation methods to establish a static NeRF, which is subsequently optimized using SDS loss derived from a video diffusion prior. Specifically, our baselines: Zero-1-to-3-V and RealFusion-V utilize Zero-1-to-3 [19] and RealFusion [25] in their static stages, respectively. Furthermore, we conduct a qualitative comparison of Animate124 with MAV3D to provide a comprehensive evaluation. This comparison focuses on the prompts and examples featured on the MAV3D website[‡], thus allowing for a detailed analysis of our ap-

---
[‡]https://make-a-video3d.github.io/

Table 1. Comparison with other methods. Across all metrics, higher scores indicate better results. **Human evaluation is shown as a percentage of majority votes favoring the baseline compared to our model in the specific setting**.

Model	CLIP Evaluation				Human Evaluation				
	CLIP-R	CLIP-T	CLIP-I	CLIP-F	Text Align.	Image Align.	Video Quality	Realistic Motion	More Motion
Zero-1-to-3-V [19]	0.8746	0.3004	0.7925	0.9663	0.1667	0.1833	0.1833	0.1750	0.2667
RealFusion-V [25]	0.8939	0.3075	0.8026	0.9691	0.2583	0.3042	0.2750	0.2625	0.4083
Animate124	**0.9311**	**0.3170**	**0.8544**	**0.9781**	—	—	—	—	—

Table 2. Ablation studies on the proposed components.

Model	CLIP-R	CLIP-T	CLIP-I	CLIP-F
w.o. 3D Prior	0.9042	0.3020	0.8141	0.9704
w.o. BalancedSampl.	**0.9377**	**0.3205**	0.8083	0.9728
w.o. SemRefine.	0.9221	0.3129	0.8331	0.9715
Animate124	0.9311	0.3170	**0.8544**	**0.9781**

proach in relation to existing methodologies.

Comparison with Baselines. In our comparative analysis, Animate124 is evaluated against two baselines, Zero-1-to-3-V [19] and RealFusion-V [25], as presented in Tab. 1 and Fig. 4. As reported in Tab. 1, Animate124 outperforms both baselines quantitatively in terms of CLIP and human evaluations. Fig. 4 illustrates that Zero-1-to-3-V [19] fails to preserve the original appearance of the reference image. For example, the first example exhibits a color shift to red, and the "accordion" in the second example is absent. RealFusion-V [25], on the other hand, exhibits inconsistencies in 3D geometry. As shown in the second example, "View 1" should represent the reference view, but the "kangaroo" is inaccurately rotated. In contrast, Animate124 successfully maintains both consistent 3D geometry and the fidelity of the reference image appearance.

Comparison with MAV3D. We compare Animate124 with MAV3D [41] on two distinct settings, as illustrated in Fig. 5. The text-to-4D generation of MAV3D relies solely on text prompts, while its image-to-4D generation exclusively utilizes the reference image as a prompt. In contrast, Animate124 leverages both the reference image and the text prompt. To facilitate a more direct comparison with the image-to-4D approach of MAV3D, we refrain from specifying motion through text in Fig. 5b and use the textual name of the object as the prompt instead. Fig. 5a demonstrates that Animate124 is capable of generating dynamic motion that aligns the protagonist with the reference image. In comparison, MAV3D (Fig. 5a) struggles to control the protagonist in the 3D video. Regarding image-to-4D generation, MAV3D fails to preserve the original appearance of the reference image, as evidenced by the flamingo's body turning black. Conversely, Animate124 successfully produces more realistic videos and consistently maintaining the appearance of the reference image. These outcomes highlight the efficacy of our method.

4.3. Ablation Studies and Analysis

Effectiveness of Semantic Refinement. Semantic refinement aims at alleviating semantic drift of the video generation model with the personalized ControlNet [50]. As shown in the 3rd and last row of Tab. 2, semantic refinement can improve the performance on text alignment, image alignment, and video consistency. The improvement in the image alignment is the most significant, further demonstrating the effectiveness of addressing semantic drift. Qualitative evaluation and the comparison with super-resolution prior are illustrated in Appendix. C.

Effectiveness of 3D Diffusion Prior. 3D diffusion prior serves as a strong supervision for the first frame, which helps to learn both geometry and texture in all three stages. In the first and last row of Tab. 2, removing the 3D prior impairs the overall geometry and thus influences all three aspects of the generated video.

Effectiveness of Temporal Balanced Sampling. Removing temporal balanced sampling leads to the first frame supervision being almost ignored in the dynamic stages. The model degenerates to text-to-4D generation with image-to-3D static initialization and semantic refinement. Therefore, this model has good text alignment but the similarity to the reference image is quite poor. In addition, this model is not consistent in 3D geometry with severe Janus problem due to the lack of guidance from the 3D diffusion prior.

5. Conclusion

We introduce Animate124, the first work to animate a single in-the-wild image into a 3D video through textual motion descriptions. With the guidance of three diffusion priors, we optimize an advanced 4D grid dynamic NeRF in a static-to-dynamic and coarse-to-fine manner. Specifically, we leverage 2D image and 3D diffusion priors to develop a static 3D scene, which is then animated with video diffusion prior. To address the semantic drift inherent in the video diffusion prior, we further proposed semantic refinement, incorporating a personalized diffusion prior as additional supervision. With the innovative three-stage framework, Animate124 is capable of producing high-quality 4D dynamic scenes from both the reference image and textual descriptions.
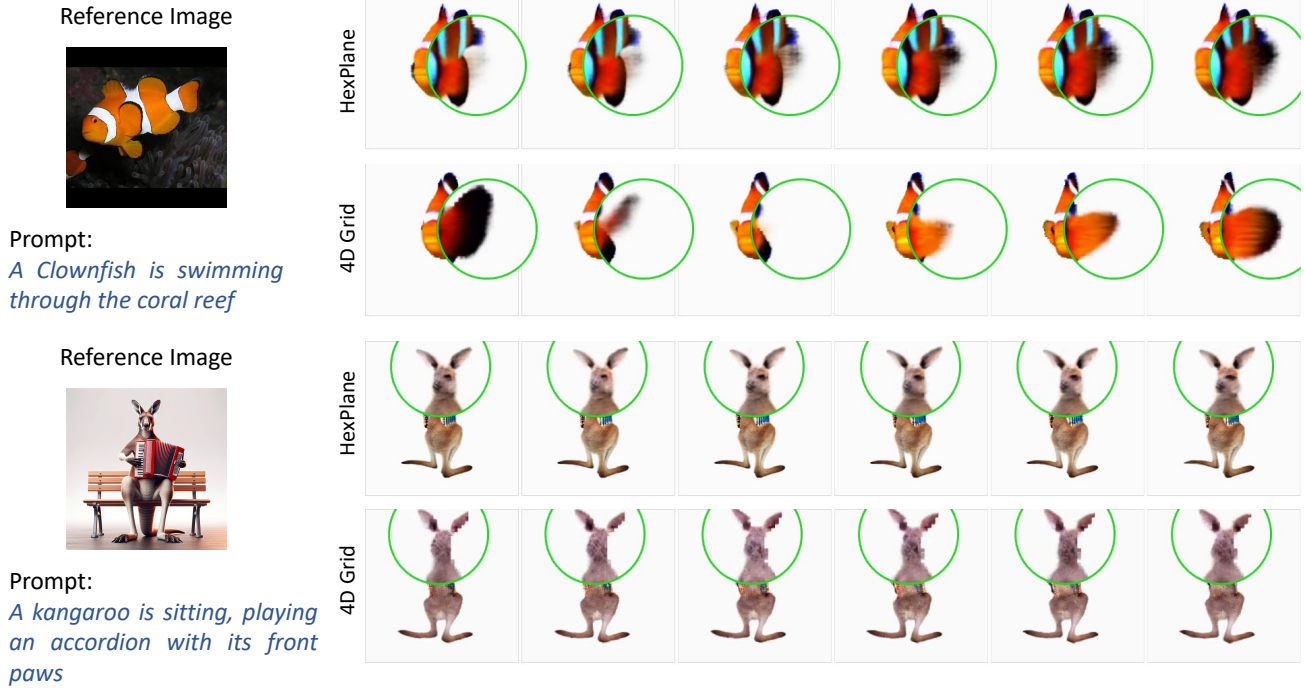
Figure 6. The comparison between 4D grid encoding and HexPlane. In each example, six consecutive frames are displayed. HexPlane is observed to struggle with limited motion and a conspicuous Janus problem.

A. Outline

- A comparative analysis of our 4D grid encoding and the HexPlane [4] dynamic NeRF backbone is presented in Sec. B;
- A comparison between our semantic refinement using ControlNet prior [50] and the refinement based on super-resolution prior is detailed in Sec. C;
- The qualitative demonstration of the effectiveness of our proposed temporal balanced sampling is provided in Sec. D.

B. Backbone

In this paper, we leverage dynamic NeRF with 4D grid encoding to represent the spatio-temporal scene. Specifically, we divide the time dimension evenly into T grids, and for each time grid, we establish a 3D multi-scale grid V. The spatio-temporal features are obtained by interpolating two nearest time grids. In contrast, MAV3D [41] employs Hex-Plane [4] dynamic NeRF for 3D video representation. This method maps the X, Y, Z, and time axes onto six 2D planes, fusing these features to calculate density and color. Our approach is directly compared with HexPlane in Fig. 6. **Note** that for HexPlane, we set the azimuth angle to $45°$ to prevent the reference camera pose from being perpendicular to one of the planes, which could result in the significant

Janus problem. The fish fin in the first example illustrates how 4D grid encoding typically exhibits more motion than HexPlane. Furthermore, the **back view** of a 4D scene in the second example demonstrates that, despite careful adjustment of the reference camera pose, HexPlane is more prone to the Janus problem compared to 4D grid encoding. Consequently, we choose 4D grid encoding for dynamic scene representation.

C. Refinement

In this paper, we introduce semantic refinement to mitigate the semantic drift associated with video diffusion models and to enhance the resolution of videos generated in the dynamic fine stage. This refinement is achieved through personalized modeling using the ControlNet [50] diffusion prior. MAV3D [41] also employs a coarse-to-fine approach, utilizing a super-resolution diffusion prior in their refinement stage to enhance results.

To assess the effectiveness of our approach in addressing semantic drift, we conduct a comparison between our personalized ControlNet prior and an image super-resolution prior[§] in Fig.7. In each example presented in Fig.7, the first row depicts the 3D video as generated in the coarse stage, while the second and third rows show the outcomes following semantic and super-resolution refinement, respectively.

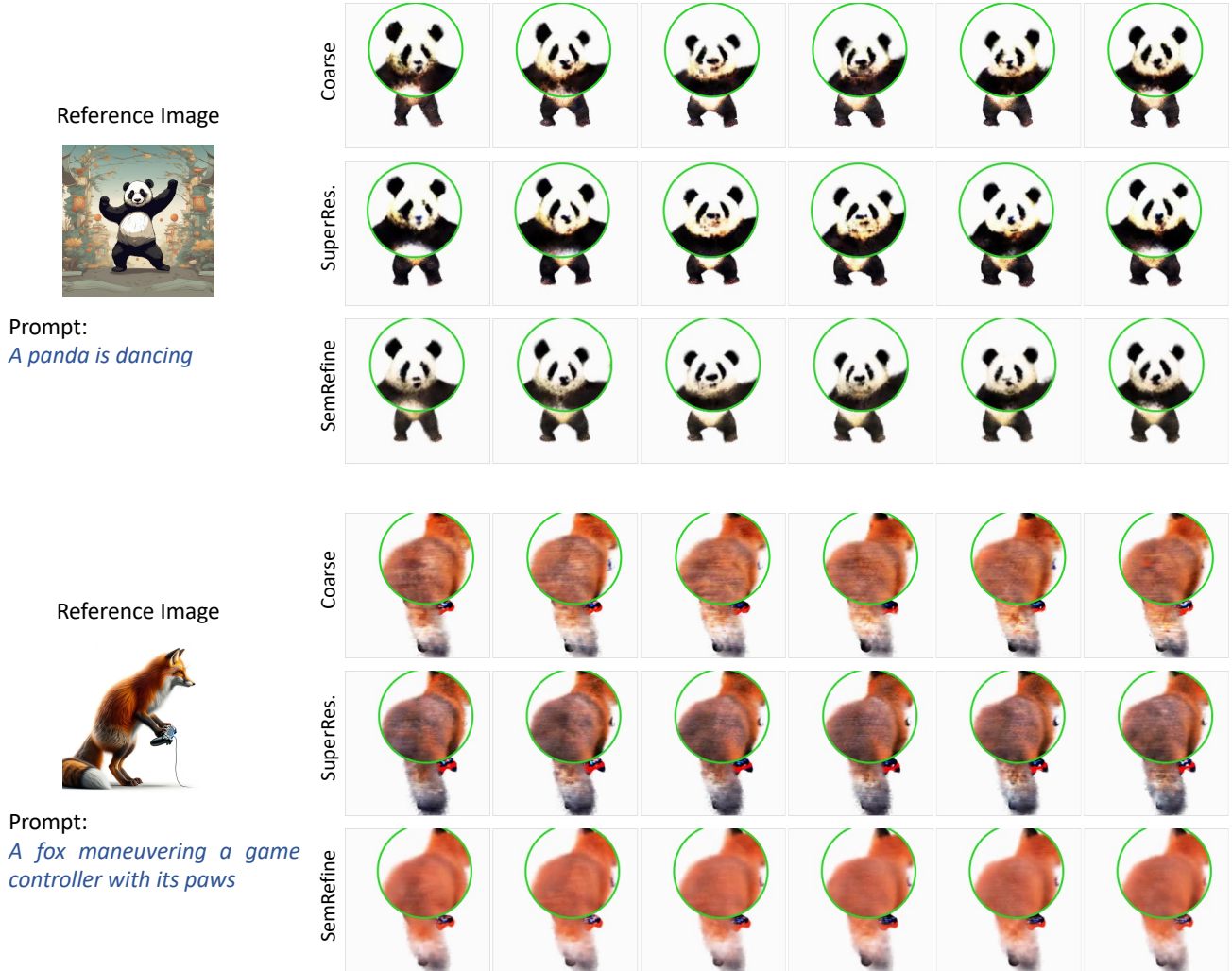[§]https://huggingface.co/stabilityai/stable-diffusion-x4-upscaler

Figure 7. The comparison between semantic refinement and super-resolution refinement in the dynamic fine stage. In each example, the first row depicts the 3D video as generated in the coarse stage, while the second and third rows show the outcomes following semantic and super-resolution refinement, respectively. Semantic refinement yields superior results by incorporating more semantic information of the reference image.

It is evident that while super-resolution can improve resolution (as seen in the fourth frame of the first example), it can also amplify errors (such as the back of the fox in the second example) present in the coarse stage, due to its lack of reference image context. In contrast, our semantic refinement not only enhances video quality but also rectifies semantic inaccuracies from the coarse stage.

D. Temporal Balanced Sampling

To enhance the supervision of the reference image and improve the learning of the initial and final time grids, we introduce temporal balanced sampling. In Fig. 8, we compare this technique with random sampling on two examples of the early timesteps. Since temporal balanced sampling can gather more information from the first frame, our method can present a more accurate appearance in the early stages.

References

[1] Jonathan T Barron, Ben Mildenhall, Matthew Tancik, Peter Hedman, Ricardo Martin-Brualla, and Pratul P Srinivasan. Mip-nerf: A multiscale representation for anti-aliasing neural radiance fields. In *CVPR*, pages 5855–5864, 2021. 2

[2] Volker Blanz and Thomas Vetter. Face recognition based on fitting a 3d morphable model. *IEEE TPAMI*, 25(9):1063–1074, 2003. 3

[3] James Booth, Anastasios Roussos, Stefanos Zafeiriou, Allan Ponniah, and David Dunaway. A 3d morphable model learnt from 10,000 faces. In *CVPR*, pages 5543–5552, 2016. 3
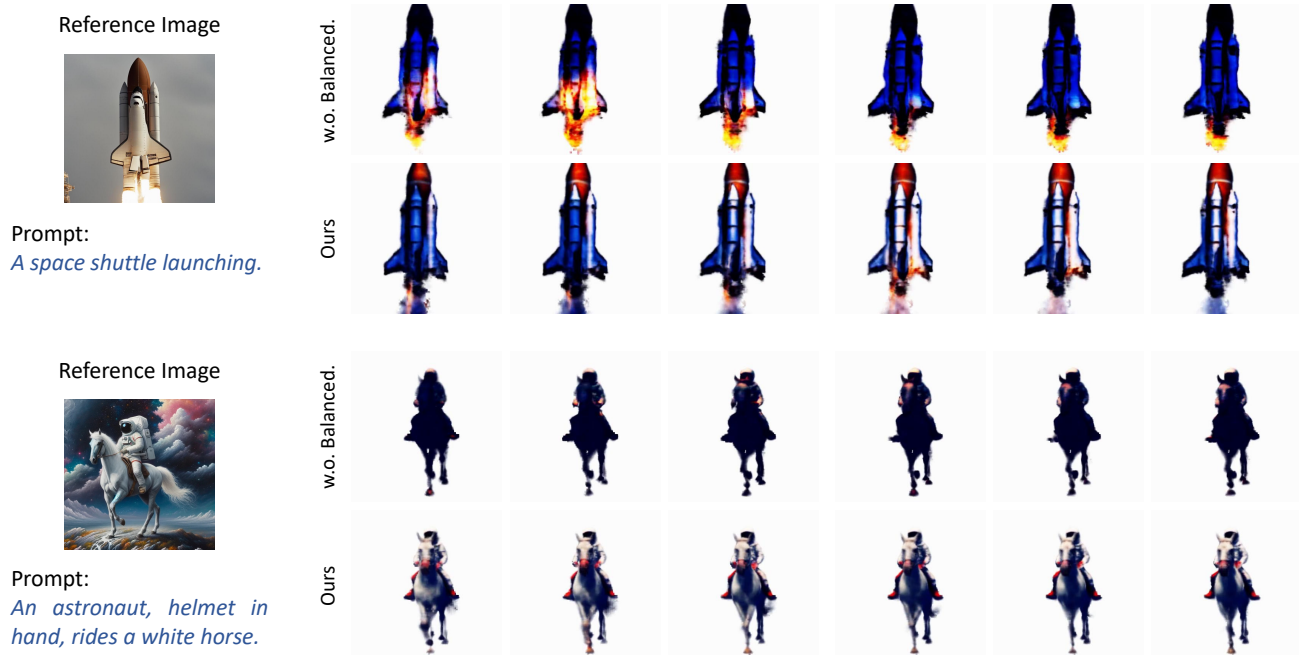
Figure 8. The comparison between the temporal balanced sampling and random sampling. In each example, we display six consecutive frames from the early timesteps. Temporal balanced sampling notably enhances the visual quality of these early frames in the videos.

[4] Ang Cao and Justin Johnson. Hexplane: A fast representation for dynamic scenes. In *CVPR*, 2023. 1, 2, 9

[5] Haoxin Chen, Menghan Xia, Yingqing He, Yong Zhang, Xiaodong Cun, Shaoshu Yang, Jinbo Xing, Yaofang Liu, Qifeng Chen, Xintao Wang, Chao Weng, and Ying Shan. Videocrafter1: Open diffusion models for high-quality video generation. *arXiv preprint arXiv:2310.19512*, 2023. 3

[6] Rui Chen, Yongwei Chen, Ningxin Jiao, and Kui Jia. Fantasia3d: Disentangling geometry and appearance for high-quality text-to-3d content creation. *arXiv preprint arXiv:2303.13873*, 2023. 3

[7] Patrick Esser, Johnathan Chiu, Parmida Atighehchian, Jonathan Granskog, and Anastasis Germanidis. Structure and content-guided video synthesis with diffusion models. In *ICCV*, 2023. 2

[8] Sara Fridovich-Keil, Giacomo Meanti, Frederik Rahbæk Warburg, Benjamin Recht, and Angjoo Kanazawa. K-planes: Explicit radiance fields in space, time, and appearance. In *CVPR*, 2023. 2, 3

[9] Rinon Gal, Yuval Alaluf, Yuval Atzmon, Or Patashnik, Amit H. Bermano, Gal Chechik, and Daniel Cohen-Or. An image is worth one word: Personalizing text-to-image generation using textual inversion. In *ICLR*, 2023. 2, 5

[10] Jonathan Ho, Ajay Jain, and Pieter Abbeel. Denoising diffusion probabilistic models. In *NeurIPS*, 2020. 6

[11] Lukas Höllein, Ang Cao, Andrew Owens, Justin Johnson, and Matthias Nießner. Text2room: Extracting textured 3d meshes from 2d text-to-image models. *arXiv preprint arXiv:2303.11989*, 2023. 1

[12] Fangzhou Hong, Mingyuan Zhang, Liang Pan, Zhongang Cai, Lei Yang, and Ziwei Liu. Avatarclip: Zero-shot text-driven generation and animation of 3d avatars. *arXiv preprint arXiv:2205.08535*, 2022. 3

[13] Lianghua Huang, Di Chen, Yu Liu, Yujun Shen, Deli Zhao, and Jingren Zhou. Composer: Creative and controllable image synthesis with composable conditions. *arXiv preprint arXiv:2302.09778*, 2023. 2

[14] Ajay Jain, Ben Mildenhall, Jonathan T Barron, Pieter Abbeel, and Ben Poole. Zero-shot text-guided object generation with dream fields. In *CVPR*, pages 867–876, 2022. 3, 7

[15] Diederik P Kingma and Jimmy Ba. Adam: A method for stochastic optimization. *arXiv preprint arXiv:1412.6980*, 2014. 6

[16] Han-Hung Lee and Angel X Chang. Understanding pure clip guidance for voxel grid nerf models. *arXiv preprint arXiv:2209.15172*, 2022. 3

[17] Chen-Hsuan Lin, Jun Gao, Luming Tang, Towaki Takikawa, Xiaohui Zeng, Xun Huang, Karsten Kreis, Sanja Fidler, Ming-Yu Liu, and Tsung-Yi Lin. Magic3d: High-resolution text-to-3d content creation. In *CVPR*, 2023. 3

[18] Minghua Liu, Chao Xu, Haian Jin, Linghao Chen, Zexiang Xu, Hao Su, et al. One-2-3-45: Any single image to 3d mesh in 45 seconds without per-shape optimization. *arXiv preprint arXiv:2306.16928*, 2023. 3

[19] Ruoshi Liu, Rundi Wu, Basile Van Hoorick, Pavel Tokmakov, Sergey Zakharov, and Carl Vondrick. Zero-1-to-3: Zero-shot one image to 3d object. *arXiv preprint arXiv:2303.11328*, 2023. 1, 2, 4, 6, 7, 8

[20] Yuan Liu, Cheng Lin, Zijiao Zeng, Xiaoxiao Long, Lingjie

Liu, Taku Komura, and Wenping Wang. Syncdreamer: Generating multiview-consistent images from a single-view image. *arXiv preprint arXiv:2309.03453*, 2023. 3

[21] Matthew Loper, Naureen Mahmood, Javier Romero, Gerard Pons-Moll, and Michael J Black. Smpl: A skinned multi-person linear model. *ACM TOG*, 34(6):1–16, 2015. 3

[22] Cheng Lu, Yuhao Zhou, Fan Bao, Jianfei Chen, Chongxuan Li, and Jun Zhu. Dpm-solver: A fast ode solver for diffusion probabilistic model sampling in around 10 steps. In *NeurIPS*, 2022. 6

[23] Zhengxiong Luo, Dayou Chen, Yingya Zhang, Yan Huang, Liang Wang, Yujun Shen, Deli Zhao, Jingren Zhou, and Tieniu Tan. Videofusion: Decomposed diffusion models for high-quality video generation. *arXiv preprint arXiv:2303.08320*, 2023. 1, 3

[24] Julieta Martinez, Rayat Hossain, Javier Romero, and James J Little. A simple yet effective baseline for 3d human pose estimation. In *CVPR*, pages 2640–2649, 2017. 3

[25] Luke Melas-Kyriazi, Christian Rupprecht, Iro Laina, and Andrea Vedaldi. Realfusion: 360{\deg} reconstruction of any object from a single image. In *CVPR*, 2023. 1, 2, 3, 5, 7, 8

[26] Ben Mildenhall, Pratul P Srinivasan, Matthew Tancik, Jonathan T Barron, Ravi Ramamoorthi, and Ren Ng. Nerf: Representing scenes as neural radiance fields for view synthesis. In *ECCV*, pages 405–421. Springer, 2020. 2

[27] Thomas Müller, Alex Evans, Christoph Schied, and Alexander Keller. Instant neural graphics primitives with a multiresolution hash encoding. In *SIGGRAPH*, 2022. 2, 3

[28] Michael Niemeyer, Jonathan T Barron, Ben Mildenhall, Mehdi SM Sajjadi, Andreas Geiger, and Noha Radwan. Regnerf: Regularizing neural radiance fields for view synthesis from sparse inputs. In *CVPR*, 2022. 3

[29] Sungheon Park, Minjung Son, Seokhwan Jang, Young Chun Ahn, Ji-Yeon Kim, and Nahyup Kang. Temporal interpolation is all you need for dynamic neural radiance fields. In *CVPR*, 2023. 3

[30] Ben Poole, Ajay Jain, Jonathan T Barron, and Ben Mildenhall. Dreamfusion: Text-to-3d using 2d diffusion. *ICLR*, 2022. 1, 2, 3, 4, 5, 6

[31] Guocheng Qian, Jinjie Mai, Abdullah Hamdi, Jian Ren, Aliaksandr Siarohin, Bing Li, Hsin-Ying Lee, Ivan Skorokhodov, Peter Wonka, Sergey Tulyakov, et al. Magic123: One image to high-quality 3d object generation using both 2d and 3d diffusion priors. *arXiv preprint arXiv:2306.17843*, 2023. 1, 2, 3, 7

[32] Alec Radford, Jong Wook Kim, Chris Hallacy, Aditya Ramesh, Gabriel Goh, Sandhini Agarwal, Girish Sastry, Amanda Askell, Pamela Mishkin, Jack Clark, et al. Learning transferable visual models from natural language supervision. In *ICML*, pages 8748–8763. PMLR, 2021. 3, 7

[33] Amit Raj, Srinivas Kaza, Ben Poole, Michael Niemeyer, Nataniel Ruiz, Ben Mildenhall, Shiran Zada, Kfir Aberman, Michael Rubinstein, Jonathan Barron, et al. Dreambooth3d: Subject-driven text-to-3d generation. *arXiv preprint arXiv:2303.13508*, 2023. 1

[34] Aditya Ramesh, Prafulla Dhariwal, Alex Nichol, Casey Chu, and Mark Chen. Hierarchical text-conditional image generation with clip latents. *arXiv preprint arXiv:2204.06125*, 2022. 1

[35] Robin Rombach, Andreas Blattmann, Dominik Lorenz, Patrick Esser, and Björn Ommer. High-resolution image synthesis with latent diffusion models. In *CVPR*, 2022. 1, 2, 3, 4, 6

[36] Nataniel Ruiz, Yuanzhen Li, Varun Jampani, Yael Pritch, Michael Rubinstein, and Kfir Aberman. Dreambooth: Fine tuning text-to-image diffusion models for subject-driven generation. In *CVPR*, 2023. 2, 5

[37] Chitwan Saharia, William Chan, Saurabh Saxena, Lala Li, Jay Whang, Emily L Denton, Kamyar Ghasemipour, Raphael Gontijo Lopes, Burcu Karagol Ayan, Tim Salimans, et al. Photorealistic text-to-image diffusion models with deep language understanding. *NeurIPS*, 35:36479–36494, 2022. 1, 3

[38] Ruizhi Shao, Zerong Zheng, Hanzhang Tu, Boning Liu, Hongwen Zhang, and Yebin Liu. Tensor4d: Efficient neural 4d decomposition for high-fidelity dynamic reconstruction and rendering. In *CVPR*, 2023. 2

[39] Uriel Singer, Adam Polyak, Thomas Hayes, Xi Yin, Jie An, Songyang Zhang, Qiyuan Hu, Harry Yang, Oron Ashual, Oran Gafni, et al. Make-a-video: Text-to-video generation without text-video data. *arXiv preprint arXiv:2209.14792*, 2022. 1

[40] Uriel Singer, Adam Polyak, Thomas Hayes, Xi Yin, Jie An, Songyang Zhang, Qiyuan Hu, Harry Yang, Oron Ashual, Oran Gafni, et al. Make-a-video: Text-to-video generation without text-video data. *arXiv preprint arXiv:2209.14792*, 2022. 4

[41] Uriel Singer, Shelly Sheynin, Adam Polyak, Oron Ashual, Iurii Makarov, Filippos Kokkinos, Naman Goyal, Andrea Vedaldi, Devi Parikh, Justin Johnson, et al. Text-to-4d dynamic scene generation. In *ICML*, 2023. 1, 2, 3, 4, 7, 8, 9

[42] Cheng Sun, Min Sun, and Hwann-Tzong Chen. Direct voxel grid optimization: Super-fast convergence for radiance fields reconstruction. In *Proceedings of the IEEE/CVF Conference on Computer Vision and Pattern Recognition*, pages 5459–5469, 2022. 2

[43] Jingxiang Sun, Bo Zhang, Ruizhi Shao, Lizhen Wang, Wen Liu, Zhenda Xie, and Yebin Liu. Dreamcraft3d: Hierarchical 3d generation with bootstrapped diffusion prior. *arXiv preprint arXiv:2310.16818*, 2023. 5

[44] Jiaxiang Tang, Jiawei Ren, Hang Zhou, Ziwei Liu, and Gang Zeng. Dreamgaussian: Generative gaussian splatting for efficient 3d content creation. *arXiv preprint arXiv:2309.16653*, 2023. 3

[45] Haochen Wang, Xiaodan Du, Jiahao Li, Raymond A Yeh, and Greg Shakhnarovich. Score jacobian chaining: Lifting pretrained 2d diffusion models for 3d generation. In *CVPR*, 2023. 3

[46] Jiuniu Wang, Hangjie Yuan, Dayou Chen, Yingya Zhang, Xiang Wang, and Shiwei Zhang. Modelscope text-to-video technical report. *arXiv preprint arXiv:2308.06571*, 2023. 2, 4

12

[47] Xiang Wang, Hangjie Yuan, Shiwei Zhang, Dayou Chen, Ji-uniu Wang, Yingya Zhang, Yujun Shen, Deli Zhao, and Jin-gren Zhou. Videocomposer: Compositional video synthesis with motion controllability. In *NeurIPS*, 2023. 2, 3

[48] Zhengyi Wang, Cheng Lu, Yikai Wang, Fan Bao, Chongxuan Li, Hang Su, and Jun Zhu. Prolificdreamer: High-fidelity and diverse text-to-3d generation with variational score distillation. In *NeurIPS*, 2023. 3, 6

[49] Dejia Xu, Yifan Jiang, Peihao Wang, Zhiwen Fan, Yi Wang, and Zhangyang Wang. Neurallift-360: Lifting an in-the-wild 2d photo to a 3d object with 360{\deg} views. In *CVPR*, 2023. 2

[50] Lvmin Zhang and Maneesh Agrawala. Adding conditional control to text-to-image diffusion models. *arXiv preprint arXiv:2302.05543*, 2023. 2, 5, 6, 8, 9

[51] Daquan Zhou, Weimin Wang, Hanshu Yan, Weiwei Lv, Yizhe Zhu, and Jiashi Feng. Magicvideo: Efficient video generation with latent diffusion models. *arXiv preprint arXiv:2211.11018*, 2022. 1